

Experimental Study of the Scouring Flow Field at the Base of Wind Turbine Mounts

D. McGovern¹., S. Ilic¹., S. J. McLelland²., A. Folkard¹., and B. J. Murphy².

¹Lancaster Environment Centre, Lancaster University, Bailrigg, Lancaster LA1 4YQ, UK
²

1. INTRODUCTION

The alteration of a flow by the presence of a vertical cylinder that spans the depth of the flow causes an increase in the fluid velocity and turbulence. The resulting flow field exhibits three-dimensionality. Such alteration can result in erosion at the base of the cylinder known as ‘scour’. Such scour can expose portions of the pile that are under the bed and adversely affect structural integrity.

This study is motivated by local scour at offshore wind turbines. To date, local scour at circular piles has been studied primarily by scale model testing. The vast majority of which is for pier scour at bridges. Comprehensive reviews of this research are given by (Breusers 1977) and (Melville 2000) for bridge piers, and (Sumer 2001) for the marine case. There is little investigation of the flow field at bridge-piers and marine structures. The marine environment has the added complexity of tidal currents and waves. The few studies of the flow field are of the unidirectional steady currents in the river environment and the majority use intrusive point measurements. In this paper, a mix of intrusive and non-intrusive measurements of velocity are used to identify the characteristics of the flow field around an offshore wind turbine mount under a tidal current. The results of rigid bed tests are given for smooth and retrofit piles. The retrofit piles are designed to suppress vortex shedding and downflow strength. These results are the precursor to mobile bed scour experiments.

Several researchers have studied the flow field around bridge piers. The early study by (Shen 1966) was the first to look at flow field at the pier and identify its characteristics. Studies by (Shen 1969), (Melville 1975), (Melville 1977), (Dargahi 1987) further identified the flow but mainly on the plane symmetry upstream of the pile. Eventually (Dey 1995) took point measurements of velocity at various radial positions around the circumference of the pier. (Graf 1999) and (Graf 2002) studied the flow field in polar coordinates, using an un-intrusive acoustic methods to identify the flow properties within, and outside the mobile and rigid bed case. (Dey 2007) investigated the flow characteristics inside the scour hole at different ‘frozen’ stages of development on the upstream side of the pier using ADV. (Ahmed 1998) conducted a series of experiments studying the flow around bridge piers in smooth, rigid and mobile bed conditions using pitch probes to measure velocity. (Sarker 1998) employed 2D Acoustic Doppler Velocimeter (ADV) along the centreline both up and downstream of cylinder. (Johnson 2003) used Particle Image Velocimetry (PIV) to give horizontal velocity fields near the free surface, and bed for a variety of water depths and flow velocities. (Roulund 2005) conducted Laser Doppler Anemometry (LDA) measurements of velocity along the plane of symmetry upstream and downstream of the pile.

The structure of the flow field around a cylinder in a marine environment is much the same as that of riverine case, (Whitehouse 1998). There has been significant attention in the literature to the case of waves and unidirectional currents in marine scour (review given by (Sumer 2001)). However, similar to the case of bridge scour, there is little investigation of the flow field of tidal currents. The flow field in waves and steady currents was investigated by ((Sumer 1992); and references therein amongst others). The author has not found any investigation of tidal currents on the flow field or scouring. (Escarameia 1998). and (Margheritini 2006) look at the scour depth and time-development in estuaries and off-shore environments respectively. For (Margheritini 2006), the tidal flow is approximated to be an equal and opposite constant velocity.

This study focuses on the influence of a tidal current on the flow field. The role of waves is not investigated. The wind generated wave boundary layer, though having a steeper velocity gradient and thus a higher bed shear, is usually not as thick as the current. In deeper water, it may not reach the bed. (Sumer 1997) conducted a series of experiments using irregular waves to avoid the formation of large bedforms with superimposed currents. It was noted that the current component of scour, that is, the horseshoe vortex and downflow was more important than the wave induced component – that caused by the steady streaming. Co-directional waves, however, have been shown to have little effect on the current at the boundary layer (Sumer 2001a), though only in terms of equilibrium scour depth.

It is noted that the ‘equilibrium scour depth’, so often used in steady current and wave scour investigations may not be as useful a measure of scour depth in an oscillating and unsteady flow environment because it represents the average depth in a highly variable system. Tidal flows act to infill to an extent, the upstream scour hole and vice versa as the flow reverses. The equilibrium scour

depth is not necessarily the maximum scour depth, nor may it be even close to that value. Thus knowing the equilibrium scour depth, but in terms of how it related to the maximum scour depth, the dynamics of the scour depth, and the points of 'high risk' in the tidal cycle in terms of high scour depth is also important. The spatio-temporal dynamics of the scour hole are an important characteristic. This is the motivation for this study. This paper will look at the three-dimensional characteristics of the flow field around a pile under a changing currents and water depths. The model is designed to be applied to off-shore wind turbines and tidal currents.

(PAPER 2)

To date, scour protection for offshore wind turbines consists of installing a hardened layer on the sea bed around the pile. This usually consists of rip-rap techniques. A better understanding of the tidal flow field should improve such protection. It is also suggested that such protection by mitigation (in-filling holes as they form), or pre-empting of scour (rip rap, mattresses) is somewhat inefficient. Better perhaps to dictate the flow field in such a way as to reduce bed shear amplification. This is not as straightforward as the bridge scour case; the current direction changes in such a way that the entire circumference of the pile needs to be included. Streamlining the pile to the flow to reduce separation is not a practical option. Sacrificial piles and sills are commonly used to protect bridge piers ((Chiew 2002) and references therein). They are placed upstream of the pier they protect and work by altering the flow field, around the pier by reducing its erosive potential. In doing so, they effectively sacrifice themselves to scour. Placing sacrificial structures around the entire circumference of a pile for tidal flow may not be as cost effective. This leaves the modification of the pier itself. The attachment of a collar, or slot through the pier is a method that is also used ((Kumar 1999) and references therein). Slots through the pile are not practical for tidal flows. The collar has proved to reduce scour ((Ettema 1980),(Kumar 1999) and references therein). These investigations are confined to clear-water scouring at bridge piers. In the atmosphere, spiral stakes are attached to smoke stacks in order to eliminate vortex shedding. The aim is to reduce vibrations on the stack. The motivation for this paper is to investigate the flow field around three different types of pile in tidal currents; a smooth pile, a collared pile and a spiralled pile.

2. EXPERIMENTAL METHOD

The experiments were conducted in the 11m long, 6m wide re-circulating flume at The Deep, University of Hull. Flow dividers were used to create a channel 1.2m wide by 11 m in length. Figure 2-1 is a schematic diagram of the experimental set-up. Unidirectional flow is provided by two 500l/s capacity electric pumps. A lattice screen at the top of the flume calms the flow on entry to the flume. The 1.2m wide channel was constructed with a raised bed formed from marine plywood drilled onto blocks of concrete. The centre of the pile was positioned at the mid-point of the flume length and width. The pile was 0.2m in diameter. A layer of pebbles were glued to the upstream end of the channel in order to help induce a boundary layer. The cylinders were sprayed with black paint to reduce light scatter.

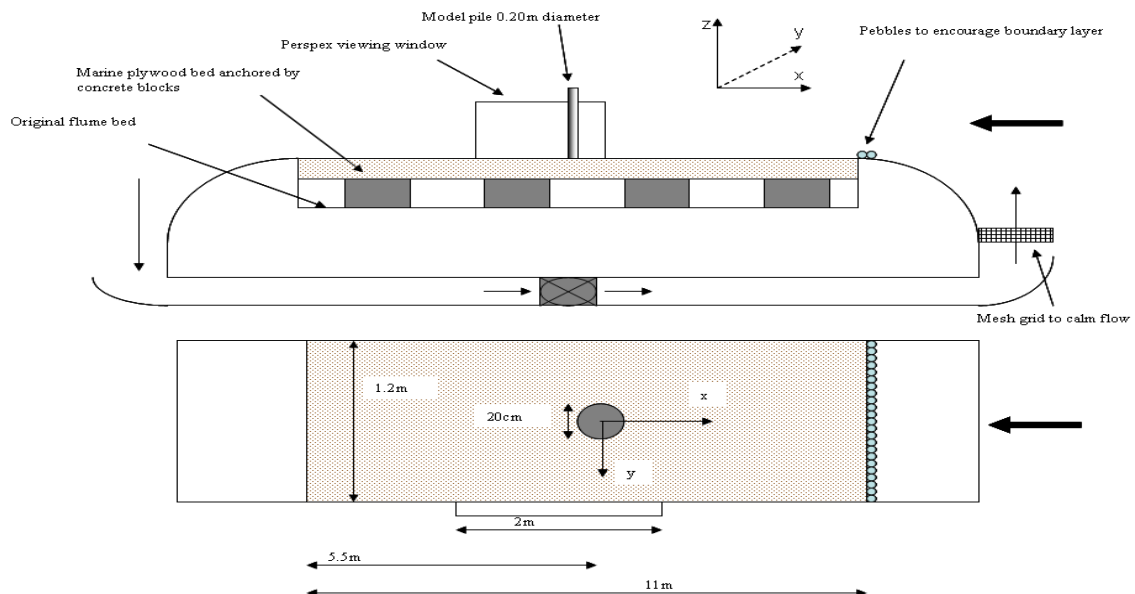


Figure 2-1. Schematic diagram of the experimental set-up

2.2 DATA AQUISITION

There are in total four methods of data collection; Stereoscopic Particle Image Velocimetry (PIV) using a Dantec instrument; Nortek Acoustic Doppler Velocimeter 3D 50hz (ADV); Nortek Acoustic Doppler Velocimeter 200Hz Vectrino; and Pressure transducers. The set-up is given in figure 2-2. Upstream of the pile, an array of four Acoustic Doppler Velocimeter (ADV) are mounted vertically on a specially made sliding mount that allows the x position to be varied from 0.013m away from the pile, to a maximum of 1.150m upstream from the pile (figure 2-3a-b). The sampling volumes of each ADV are positioned at $y = 0, +0.12, +0.17, +0.22$ m. The Vectrino sampled at various positions in x and y that spanned the shaded area in figure 2-2. The red dots in figure 2-2 show the positions of 24 fixed pressure transducers. The PIV was set-up to capture verticle slices of the flow field in downstream of the pile at four different y positions. At positions $y=0$ four ‘slices’ of the flow field were captured at $x=0\text{m}-0.5\text{m}, 0.5\text{m}-1\text{m}, 1\text{m}-1.5\text{m}$ and $1.5\text{m}-2\text{m}$.

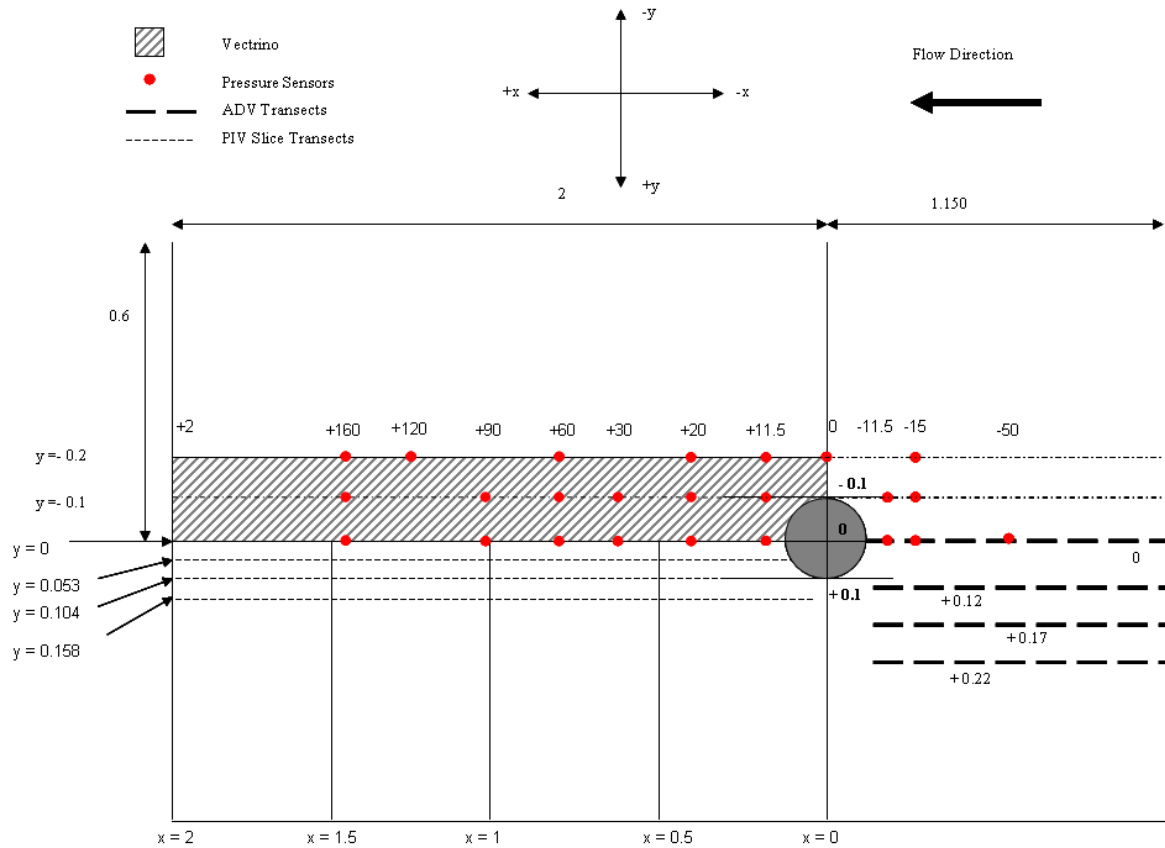


Figure 2-2. Schematic top-down view of the experimental set-up showing the ADV positions (thick striped lines), Vectrino positions (shaded striped area), Pressure sensor positions (red dots), and the PIV slice positions (thin striped lines).

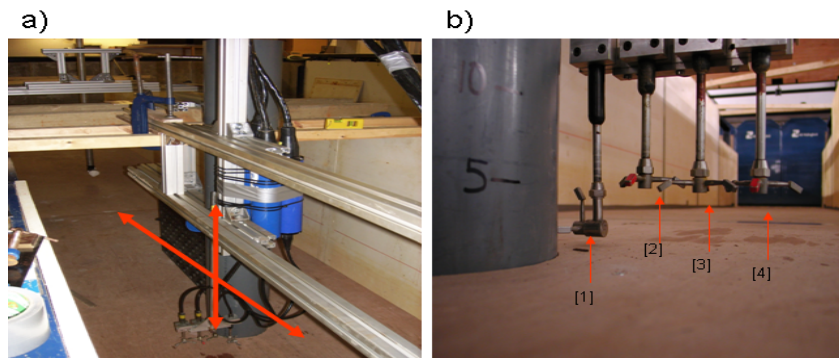


Figure 2-3a-b. Images of the ADV rig upstream of the pile. a) image taken looking downstream; the red arrow indicates the ability to slide the rig in both the x and z direction in order to capture full profiles at various positions x. b) Close up image of

the transducer configuration. The side-looking ADV [1] is positioned as such that the sampling volume is directly on the centreline. The three down-looking ADV [2-4] sample at $y=+0.12, +0.17$ and $+0.22\text{m}$.

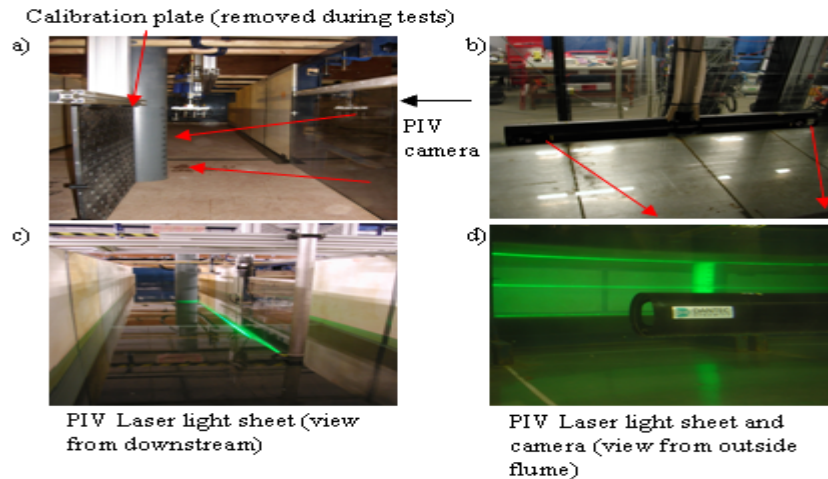


Figure 2-4 a-d. a) image of the pile, calibration plate and Perspex screen taken from downstream. b) the DANTEC CCD Digital camera pair. The red arrows in a) and b) indicate the direction of image capture. This image is taken from within the flume looking outwards towards the side. c) the laser firing downstream of the pile. d) the laser firing with the camera in the foreground. Image taken outside of the flume.



Figure 2-5 a-c. a) image from upstream of the pressure sensor pads embedded in the plywood board. c) image showing the underside of the board. c) image showing the hole in which the cabling is fed out of the flume

2.3 PARTICLE IMAGE VELOCIMETRY

A Dantec Stereoscopic Particle Image Velocimetry (PIV) system was used to capture 3D velocity field slices. Two Charged Couple Device (CCD) digital cameras capture two consecutive images of the seeded flow (seed with Timorol of 7microns) at different angles at a rate of 15Hz for two minutes. This makes up a 'slice'. The laser is fired as a pulse meaning it fires twice 15 times per second for two minutes. The image pairs are drawn from this pulse which gives 15 per second, and thus 1800 image pairs per slice. The program Dantec Flow Manager is to process the image pairs. The software compares the position of thousands of individual seeding particles in the first image of a pair (image A) with their position in the second, (image B). From each image pair a 3D vector map is constructed, giving 1800 vector maps per slice in time series. A statistical vector map is then given for the time-averaged flow field. (Adrian 1991) provides a detailed description of the PIV technique for reference. The PIV was calibrated at the start of the experiment, and re calibrated near the end of the experiment to cater for any offset brought about by movements in the structure of the flume.

2.4 EXPERIMENTAL PROCEDURE

A total of eight experiments were performed; the parameters of which are shown in table 2-1. The tests were run in alphabetical order as they appear in table 2-1. Table 2-2a-b shows the measurements campaign for each test.

Table 2-1. Test conditions.

Test	Pile	U	H	Re _D	Fr	U _c	U/U _c
LFP1A	1	0.22	0.28	3.24E+04	0.13	0.27	0.81
LFP1B	1	0.33	0.25	4.85E+04	0.21	0.27	1.23
LFP1C	1	0.23	0.1	3.38E+04	0.23	0.26	0.87
LFP1D	1	0.15	0.4	2.21E+04	0.08	0.29	0.52
LFP2G	2	0.23	0.1	3.38E+04	0.23	0.26	0.87
LFP2E	2	0.33	0.25	4.85E+04	0.21	0.27	1.23
LFP3F	3	0.33	0.25	4.85E+04	0.21	0.27	1.23
LFP3H	3	0.23	0.1	3.38E+04	0.23	0.26	0.87
LFP0W	0	0.23	0.1	3.38E+04	0.23	0.26	0.87
LFP0X	0	0.33	0.25	4.85E+04	0.21	0.27	1.23
LFP0Y	0	0.22	0.28	3.24E+04	0.13	0.27	0.81
LFP0Z	0	0.15	0.4	2.21E+04	0.08	0.29	0.52

Table 2-a. Measurement campaign.

a)

Test	ADV	Vectrino	PIV	Pressure Sensor
LFP1A	1	1	1	n/a
LFP1B	2	2	2	n/a
LFP1C	2	2	2	n/a
LFP1D	2	2	2	n/a
LFP2G	2	2	2	n/a
LFP2E	2	2	2	n/a
LFP3F	2	2	2	n/a
LFP3H	2	2	2	n/a
LFP0W	2	2	2	n/a
LFP0X	2	2	2	n/a
LFP0Y	2	2	2	n/a
LFP0Z	2	2	2	n/a

b)

ADV1		ADV2		PIV1		
measurement time	x positions of profiles (m)	measurement time	x positions of profiles (m)	Measurement Time	Y positions (m)	X Positions (m)
2min	-0.133	2min	-0.133	2min	0	0-0.5, 0.5-1, 1-1.5, 1.5-2
2min	-0.175	2min	-0.145	2min	0.053	0-0.5, 0.5-1
2min	-0.225	2min	-0.155	2min	0.104	0-0.5, 0.5-1
2min	-0.275	2min	-0.165	2min	0.158	0-0.5, 0.5-1, 1-1.5, 1.5-2
2min	-0.325	2min	-0.175	2min	0.365	0-0.5, 0.5-1, 1-1.5, 1.5-2
2min	-0.4	2min	-0.2	PIV2		
2min	-0.5	2min	-0.25	Measurement Time	Y positions (m)	X Positions (m)
2min	-0.6	2min	-0.325	2min	0	0-0.5, 0.5-1, 1-1.5, 1.5-2
2min	-0.7	2min	-0.5	2min	0.053	0-0.5, 0.5-1
2min	-0.9	2min	-0.7	2min	0.104	0-0.5, 0.5-1
2min	-1.15	2min	-1.15	2min	0.158	0-0.5, 0.5-1, 1-1.5, 1.5-2
Vectrino1		Vectrino2				
measurement time	x positions of profiles (m)	measurement time	x positions of 3 point profiles (m)	measurement time	positions of profiles (r)	x positions of profiles
5min	0.3	5mins	0.3	10mins	0	300
5min	0.4	5mins	0.4	10mins	-0.1	300
5min	0.5	5mins	0.5	10mins	-0.2	300
5min	0.6	5mins	0.6	10mins	0	1000
5min	0.9	5mins	0.7	10mins	0	2000
5min	0.12					
5min	0.16					
5min	0.2					

The experimental procedure is as follows:

- i.) The flume was filled to the required water depth. The required depth was measured by a tape placed on the side of the flume, and with an accuracy of +/- 7mm using the pressure sensors.
- ii.) When the required depth was reached, one of the two pumps was activated. The discharge was attained by adjusting the rate Hz of the pump and by fluttering the control valve for minor adjustments. The required flow velocity was gauged by the ADV array upstream set at $0.4z_0$ at the x position furthest from the pile ($x=1150$). From analysis of profiles on the centreline and off for both pile and no pile scenarios show the velocity profile at this point to be well formed and reasonable logarithmic. Measurements were also taken by the Vectrino at its most downstream position and off the centreline. Due to the nature of the pumps it was very difficult to give a constant discharge at such low fraction of their capacity and the velocity was found to fluctuate about the required value. Every attempt was made to keep this below +/- 3cms. There was no way of knowing the exact free stream velocity during tests.
- iii.) PIV measurements were then taken. First at $y=0, x=0$, then at each change in x position required before the light sheet was moved to the next y position and the required slices taken. This was continued until all PIV was complete for that test. During PIV capture, the pressure sensors were also collecting data in various measurement suites.

- iv.) The upstream ADV and Vectrino were then taken after PIV as the seeding particles are far larger than the PIV meaning they would interfere with measurements if in the flow during PIV capture. ADV and Vectrino were taken simultaneously. They were positioned manually for each required x / y position. To ensure minimal interference of the upstream ADV profile in the flow to the Vectrino reading downstream, the sampling was taken in a way that the distance between the two instruments was always at a maximum. There is, however, a certain amount of interference in any case.
- v.) Once the measurement campaign is completed for a test the pumps are turned off and the flume is filled/drained to the next height. Depending on the amount of suspension of seeding material in the flow, the flume may be drained to the ‘lip’ of the tank (i.e., water only remains in the reservoirs at the tank ends) and manually cleaned. In some cases it will have to be fully drained and refilled. If draining to a lower depth, the ADV suit may be completed first before fully draining, cleaning and re-filling the flume, depending on the condition of the water. As such, this seemingly ad hoc way of completing the measurements was justified as it was the most efficient way of using the allotted time in the flume.

2.5 SCALING

The prototype / model conditions are set out in table 2-3. The tide was progressive with a maximum $U = 1$ m/s, mid water depth was 5m and tidal range 6m. The diameter of the pile was 4m. In the model the tide was divided into three velocity-depth values (time-steps) that corresponded to clear water, transitional and live bed regime, with LFP1A as a Froude scaled test. The scale was 1:20.

Table 2-3. Model – prototype comparison.

Parameter	Units	Prototype	Scaled Model	Time step		
				1	2	3
U	m/s	1	0.22	0.15	0.33	0.23
D	m	4	0.2	0.2	0.2	0.2
H	m	5	0.28	0.4	0.25	0.1
Fr		0.14	0.13	0.08	0.21	0.23
Re _D		2.94E+06	3.24E+04	2.21E+04	4.85E+04	3.38E+04
U/U _c		1.76	0.97	0.71	1.20	0.88

This approach allows the dynamics of the flow intensity (U/U_c) regimes to be investigated, behind this is that a key difference in tidal scour to unidirectional scour is the dynamics of the flow intensity regimes.

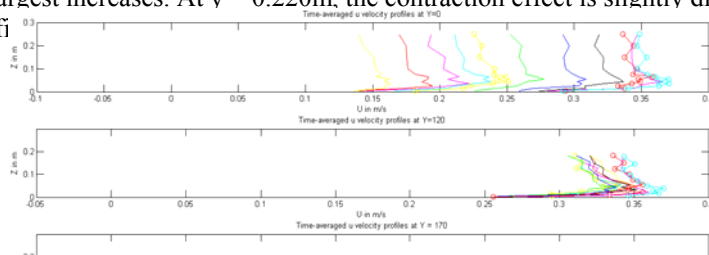
2.5.1 THE BLOCKAGE EFFECT

According to (Whitehouse 1998), the blockage effect is insignificant as long as the pile diameter to flume width ratio is $\leq 1/6$. The pile diameter in this experiment is quite large, though this does not cause problems and measurements of the flume indicate that there is no significant adverse effect. The large pile diameter allows larger Re_D to be investigated at these velocities.

3 EXPERIMENTAL RESULTS

3.1 VELOCITY FIELDS

Figure 3-1 presents the profiles of velocity component u for the test $U=0.33$ m/s, $H=0.25$ m (LFP1B) along the centreline at $y=0$. This corresponds to mid tide time step. The u component of velocity shows distinctly the retardation effect of the pile on the centreline. The effect of the pile is felt upstream up to $x = -0.325$ m ($x/D = 1.625$). The next profile, at $x=-0.500$ ($x/D = 2.5$) seems to be approximately the same as the undisturbed values. $x/D = 1.625$ is a smaller reach than suggested in (Sarker 1998) ($x/D \sim 6$). Off the centreline at $y = 0.120$ m the slowing effect is dramatically reduced, though the distance at which the flow ‘feels’ the pile is similar (somewhere in between $x = -0.325$ m ($x/D = 1.625$) and $x = -0.500$ ($x/D = 2.5$)). Profiles $x=-0.133$ ($x/D = 0.66$) to $x=-0.165$ ($x/D = 0.825$) exhibit a small increase in u , presumably due to the contraction effect of the pile. This effect is even more apparent at $y = 0.170$ m, where velocity is raised upto 0.05m/s faster than the undisturbed value. This effect is present on profiles $x=-0.133$ ($x/D = 0.66$) to $x=-0.200$ ($x/D = 1$) with $x=-0.133$ ($x/D = 0.66$) and $x=-0.145$ ($x/D = 0.725$) exhibiting the largest increases. At $y = 0.220$ m, the contraction effect is slightly diminished, although the same profi



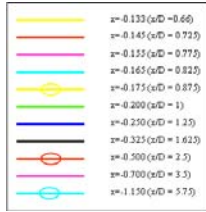


Figure 3-1. Profiles of u velocity from LFP1B at $y = 0 - 220$.

Figure 3-2 presents profiles of v for the same test. At $y = 0\text{m}$, the values are less than 0.05m/s across the profiles. Upstream of $x = -0.250$ ($x/D = 1.25$), there seems to be significant spanwise velocity near the bed, particularly in $x = -0.700$ ($x/D = 3.5$) and $x = -1.150$ ($x/D = 5.75$). This is theorised to be an artefact of the flume or ADV. From $x = -0.200$ ($x/D = 1$) and closer, the v component begins to show signs of deflection. The fact that deflection is detected means that the ADV probe is reading a fraction off the centreline, and is picking up deflection around the other side of the pile ($y = -ve$). At $y = 0.120\text{m}$ the deflection is clear. The farthest profile to feel this effect is $x = -0.325$ ($x/D = 1.625$) – notably the same as for u . Closer to the pile, for profiles $x = -0.133$ ($x/D = 0.66$) and $x = -0.145$ ($x/D = 0.725$), v appears to increase with depth with the maximum values at the bed. The max value $\sim 0.14\text{m/s}$ for $x = -0.133$ ($x/D = 0.66$)

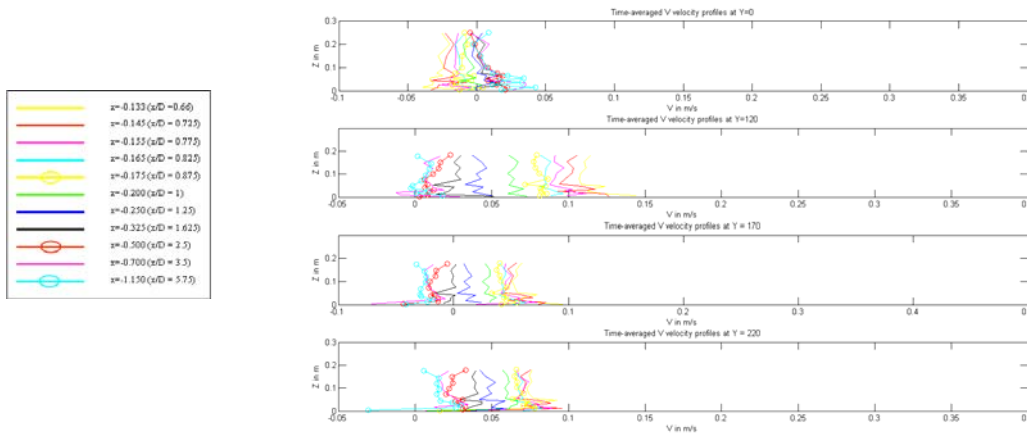


Figure 3-2. Profiles of v velocity from LFP1B at $y = 0 - 220$.

Farther away from the pile the profile is approximately uniform. The shape of the $x = -0.133$ ($x/D = 0.66$) and $x = -0.145$ ($x/D = 0.725$) v profiles are likely brought about from the deflection of fluid originally in the downflow, which also increases in strength with depth, as it is forced first to the bed, then around the pile. Such fluid will have the high energy. At $y = 0.170\text{m}$ the profiles behave in a similar manner as $y = 120$, expect that $x = -0.250$ ($x/D = 1.25$) seems to be the profile that first exhibits deflection. The maximum value is 0.05m/s slower than at $y = 120$, but is at the same point, (i.e, at the bed), nearest the pile. The profiles at $y = 220$ show deflection in a similar manner to $y = 170$.

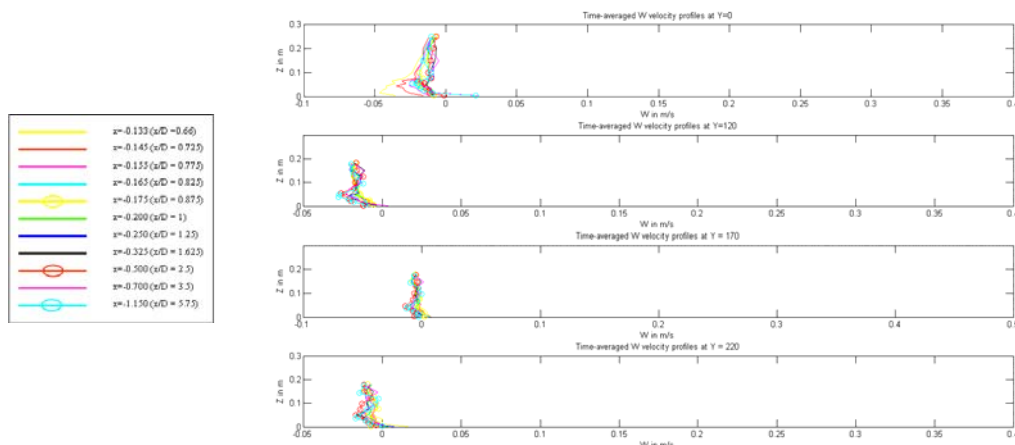


Figure 3-3. Profiles of v velocity from LFP1B at y = 0 – 220.

Figure 3-3 presents profiles of w velocity at y = 0, 120, 170 and 220. The presence of the downflow is clear at y = 0 in profiles x=-0.133 (x/D =0.66) and x=-0.145 (x/D = 0.725), the two closest to the pile. It seems that the downflow confined to within two centimetres from the pile surface. At y = 120, the downflow is no longer present. There are small values of negative w velocity, but these remain approximately constant with x and do not seem to be induced by the pile. At y = 170 there is no appreciable influence on w velocity by the pile. The profiles at y = 220 are also unaffected, apart from a slight up flow near the bed in x=-0.133 (x/D =0.66).

Figure 3-4 compares u profiles for tests for the tidal cycle: LFP1B-D b-d, where in b) U = 0.33, H = 25, c) U = 0.23, H = 0.1 and d) U = 0.15, = 0.4. The retardation of u on approach to the pile is similar throughout the tidal cycle. The structure of the profile is retained on approach to the pile. The value of u is lowered by the greatest amount (~0.2m/s) in LFP1B from the undisturbed value. LFP1C shows a decrease of approximately 0.13m/s and LP1D a decrease of 0.09m/s. it there for seems that there is a lowering in the retardation effect with water depth.

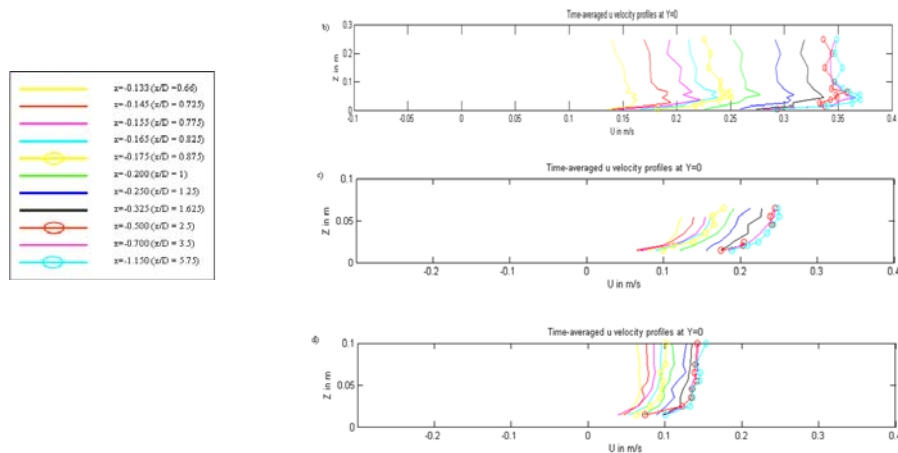


Figure 3-5. Profiles of v velocity from LFP1B - D at y = 0.

Figure 3-5 compares the v profiles for tests LFP1B-D. All show that v is essentially constant with depth. As discussed earlier, the ADV sampling volume may be slightly off the centreline, resulting in the recording of v component near the pile, particularly on LFP1B and C. LFP1D shows very little v component throughout the x limit

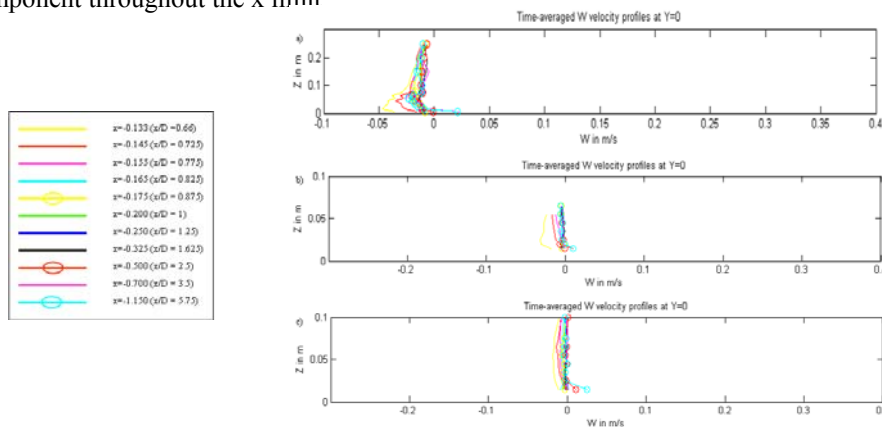


Figure 3-6. Profiles of w velocity from LFP1B - D at y = 0.

Figure 3-6 compares w profiles for tests LFP1B-D. The downflow is present in LFP1B and C at $x=-0.133$ ($x/D=0.66$) with maximum values above the lowest point in the profile of ~ 0.05 and ~ 0.035 m/s respectively. The presence of the bed presumably slows the downflow resulting in negative gradient in velocity with height near the bed. The downflow is apparent in the profiles $x=-0.133$ ($x/D=0.66$), $x=-0.145$ ($x/D=0.725$) and $x=-0.155$ ($x/D=0.775$) in LFP1B. Its range is the same in LFP1C, but the velocities at $x=-0.145$ ($x/D=0.725$) and $x=-0.155$ ($x/D=0.775$) are barely raised from the undisturbed value. LFP1D shows that there is a slight increase in velocity and the profile structure is almost linear. This may indicate that the adverse pressure gradient is not as strong as in the other time steps.

3.2 TURBULENCE FIELDS

Figure 3-7 shows plots of Turbulent Kinetic Energy (TKE) for LFP1B. It is apparent that on approach to the pile TKE drops. Figures 3-7 to 3.14 display TKE, mean turbulence intensities $[(1/3)*(\sqrt{u'u'^2}) + (\sqrt{v'v'^2}) + (\sqrt{w'w'^2})]$, Mean turbulence intensity components $[\sqrt{u'u'}]$, $[\sqrt{v'v'}]$, $[\sqrt{w'w'}]$, and corresponding contour plots. TKE decreases in value on approach to the pile from figure 3-7. As from TI plots figure 3-9 – 3-11, the u' component of the flow is by far the most dominant in the approach to the pile. Thus TKE follows a similar pattern to u as it approaches the pile.

From figure 3-8 it is apparent that there is a decrease in TI on approach to the pile. Closer to the pile, particularly on profiles $x=-0.133$ ($x/D=0.66$) and $x=-0.145$ ($x/D=0.725$), TI increases closer to the bed, presumably indicating the presence of separation. Figure 3-15 allows comparison of the spatial distribution of TKE and TI along the y coordinate.

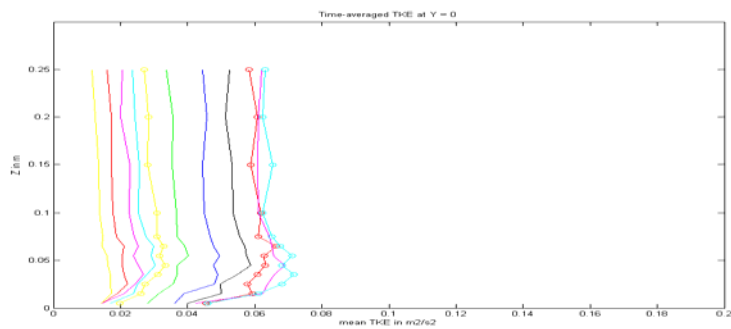


Figure 3-7. Profiles of TKE from LFP1B at $y = 0$.

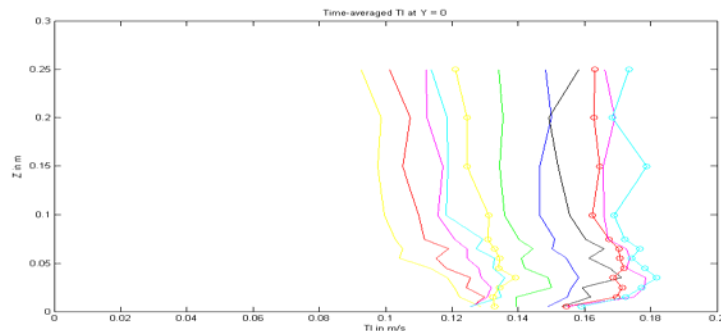


Figure 3-8. Profiles of TI $(1/3) * (\sqrt{u'u'^2}) + (\sqrt{v'v'^2}) + (\sqrt{w'w'^2})$ velocity from LFP1B at $y = 0$.

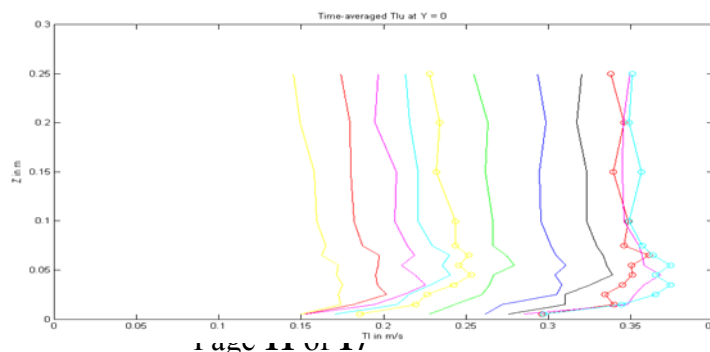


Figure 3-9. Profiles of TIu from LFP1B at $y = 0$.

Figure 3-9. Profiles of Tlu ($\sqrt{\text{mean}(u'u')}$) velocity from LFP1B at $y = 0$.

Figures 3-10 – 3-13 present TKE and TI at $y = 0$ to 120. The affect of the pile is similar to the velocity profiles. The drop in turbulence is felt only slightly on approach to the pile. It drops far less for each of profiles $x=-1.150$ ($x/D = 5.75$) to $x=-0.155$ ($x/D = 0.775$) and begins to increase from $x=-0.155$ ($x/D = 0.775$) to $x=-0.133$ ($x/D = 0.665$). This reinforces the short range effect of the pile off the centreline. The increase in TKE and TI closer to the pile is a result of the contraction of the flow. The contraction is evidently stronger and begins farther upstream of the pile from the profiles in figure 3-12 and 3-13.

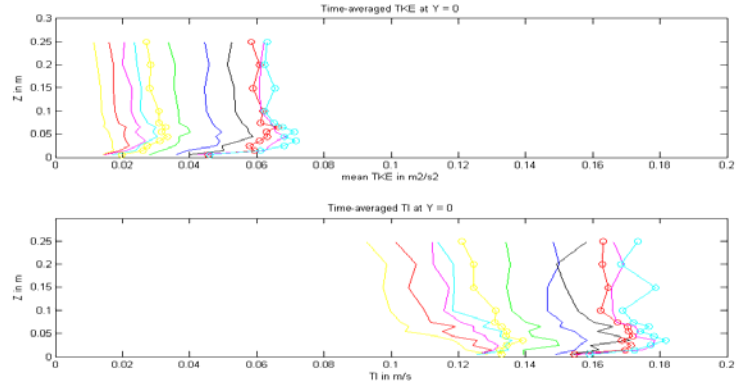


Figure 3-15. Profiles of TKE and TI from LFP1B $y=0$.

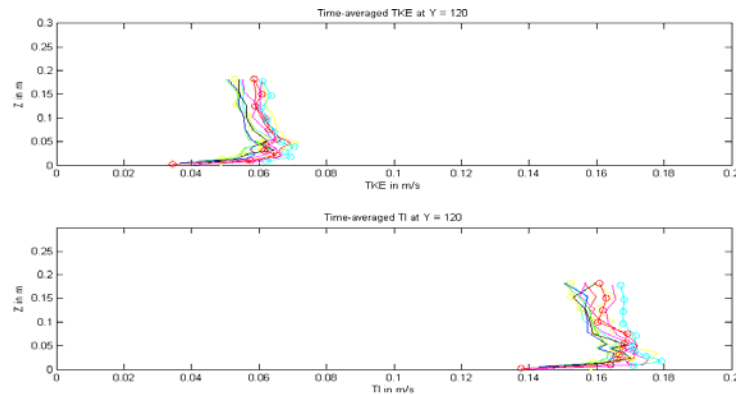


Figure 3-16. Profiles of TKE and TI from LFP1B $y=120$.

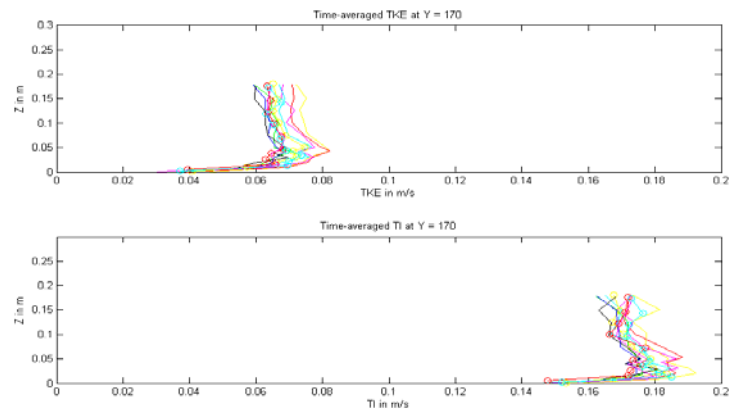


Figure 3-17. Profiles of TKE and TI from LFP1B $y=170$.

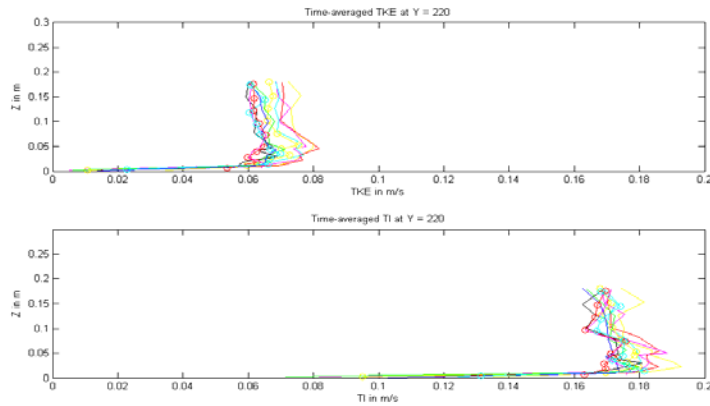


Figure 3-18. Profiles of TKE and TI from LFP1B y= 220.

3.2 PARTICLE IMAGE VELOCIMETRY

Figures 3-19 – 3-24 present 3D vector map and bed shear stress values for the flow field directly behind piles 1, 2 and 3 on the centreline for tests LFP1B, LFP2E and LFP3F. The vector maps give the v component of velocity in the form of the coloured contours. The vectors represent the w component. The vector maps are time-averages of the flow over the two minute sampling period.

Figure 3-19 presents time-averaged 3D vectors of LFP1B directly behind the pile at $y=0$. Test conditions are $U=0.33\text{m/s}$, $H=0.25$ and the pile is smooth. The main features are the reversal and stagnation point. The stagnation point is not vertical, it is approximately at $x=0\text{mm}$ at $H=-150\text{mm}$. It moves in an approximate linear fashion with height. At $H=0\text{mm}$, it is positioned at approximately at $x=50\text{mm}$. At $H=100\text{mm}$, it occurs at $x=125\text{mm}$. The v component in velocity is fairly small. The flow begins to move away from the pile just after stagnation at $x=0$ onwards. Here there are the largest vectors, and plots of bed shear stress in figure 3-20 indicate that there may be increased sediment transport here. Bed shear stress increases to a maximum of approximately 12 N m^{-2} and then begins to fall. w is generally small, but notably upward near the bed. The reversal forms part of the vortex that will be formed from separation at the pile sides.

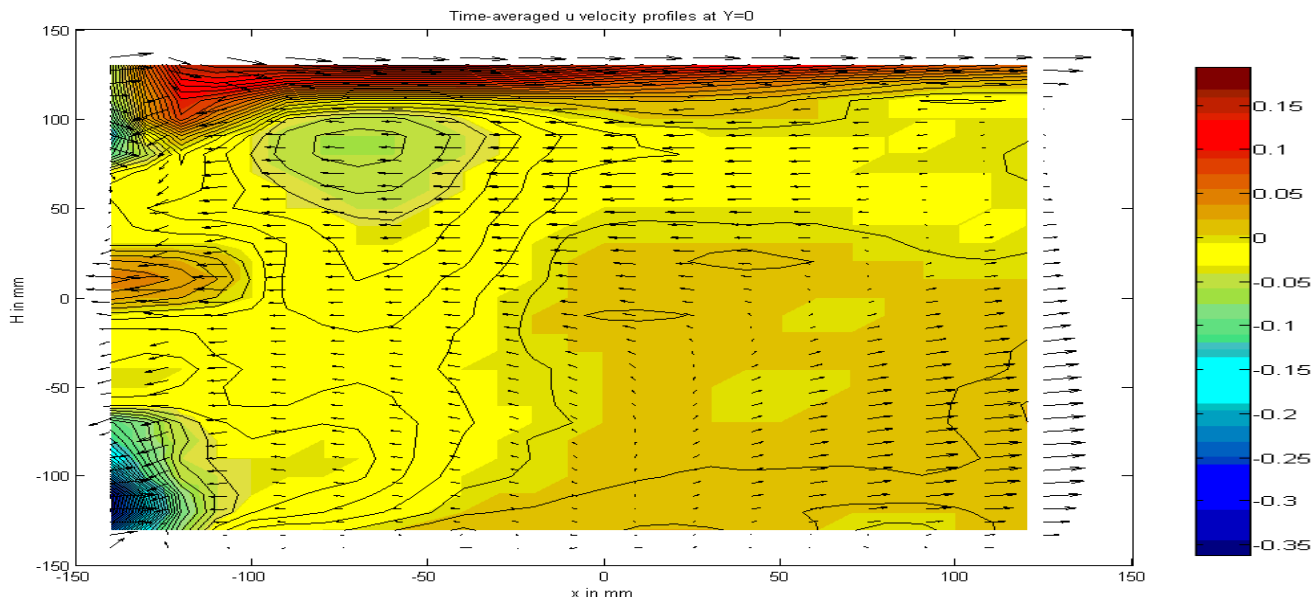


Figure 3-19. 3D vector statistics for directly behind the pile at LFP1B. The flow map is approximately 0.28 by 0.28m. The first three values from the left should be ignored as this is the location of the pile.

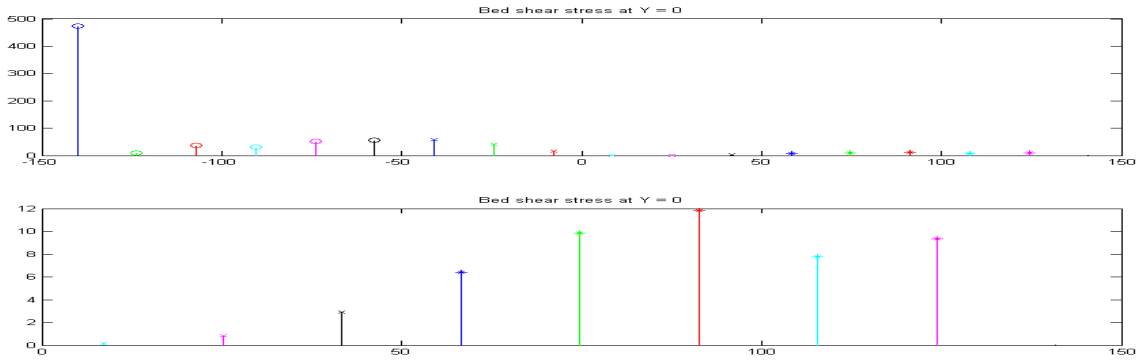


Figure 3-20a-b. Bed shear stress values at the bed relating to the equivalent profiles in figure 3-24 (figure 3-20a), directly behind the pile at LFP1B. In figure 3-20b the profiles after the point of separation only are displayed. These are the profiles that show logarithmic behaviour, and thus are the most likely to be approximately correct with the logarithmic method used. The first three values from the left of figure 3-20a should be ignored as this is the location of the pile.

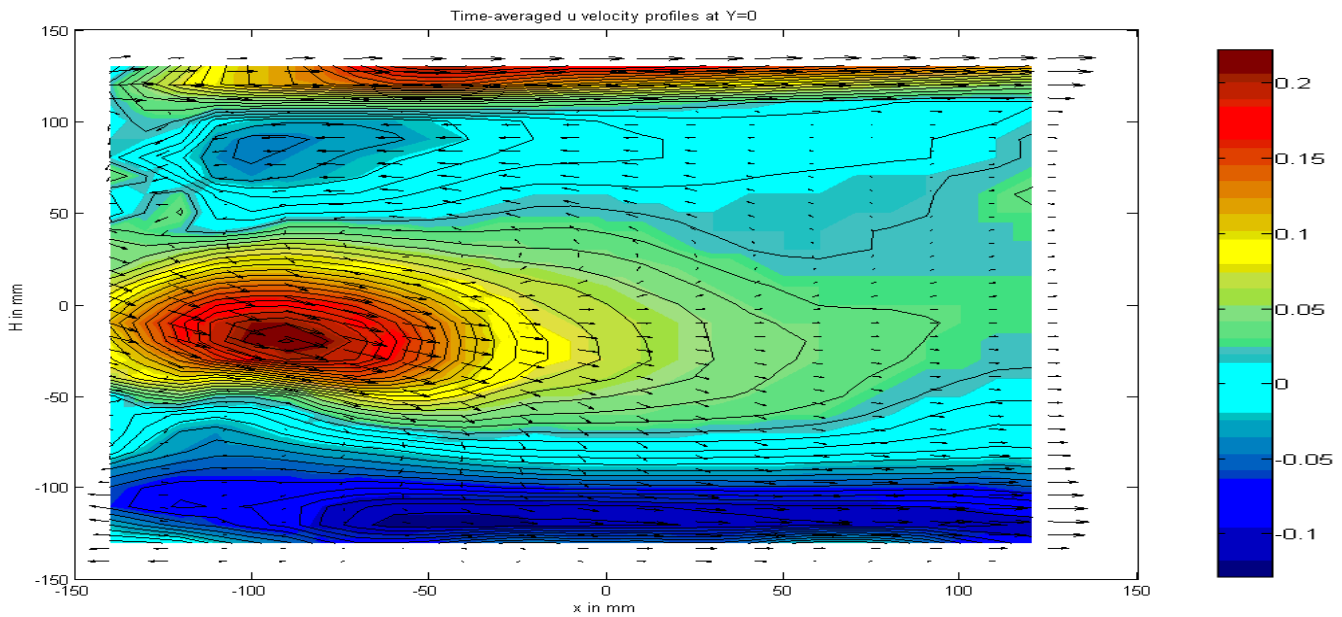


Figure 3-21. 3D vector statistics for directly behind the pile at LFP1E (spiralled pile). The flow map is approximately 0.28 by 0.28m. The first three profiles from the left should be ignored as this is the location of the pile.

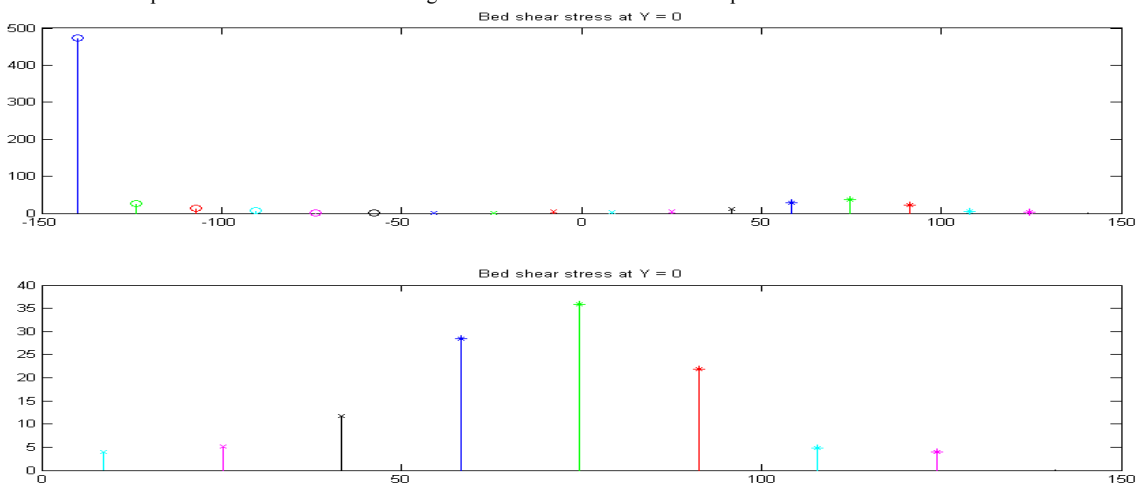


Figure 3-22a-b. Bed shear stress values at the bed relating to the equivalent profiles in figure 3-21 (figure 3-22a), directly behind the pile at LFP1E. In figure 3-22b the profiles after the point of separation only are displayed. These are the profiles that show logarithmic behaviour, and thus are the most likely to be approximately correct with the logarithmic method used. The first three values from the left of figure 3-22a should be ignored as this is the location of the pile.

Figure 3-23 presents time-averaged 3D vectors for LFP2E directly behind the pile at $y=0$ under the same test conditions as figure 3-19. The structure of the flow field is very different. The stagnation and reversal no longer exists as in figure 3-19. The main feature is a large vortex positioned just off the surface of the pile, which dominates the low field at this point. The axis of rotation appears to be in y (into the page, horizontally), which is different from the smooth pile flow field, which is in z (vertical, see figures 3-19). There is a significant v component to the flow field, which has a maximum value of approximately $2/3$ the undisturbed velocity. The range of v velocity is 0.35 m/s. This is perhaps caused by separation off the spiral sheet, which causes the flow to bend inward. The bed shear values for the spiralled pile (figure 3-22a-b) show that it may act to increase bed shear. Spiral strakes are used commonly to suppress vortex shedding induced structural vibrations in the atmosphere; however, they also act to increase drag.

Figure 3-23 and 3-24a-c present the time-averaged 3D vectors for LFP2E directly behind the pile at $y=0$, and respective bed shear stress values under the same test conditions as figure 3-19. The flow field around the ringed pile is similar to that of the spiralled pile. The dominant feature is a vortex positioned well above the bed that rotates on the y axis. There is again a large v component of flow underneath the vortex next to the pile at the bed. The range of v velocity is 0.45 m/s, with a core of maximum velocity below the vortex of approximately 0.23 m/s. It seems a lot of energy is manifest in the v component. As the flow recovers farther downstream, the u component becomes dominant with little variation in v . In this slice, u and v change in strength at the same points. The values of bed shear stress are similar to figure 3-19, which is promising, particularly is the rings act to decrease bed shear at the front and sides of the pile, as well as the rear.

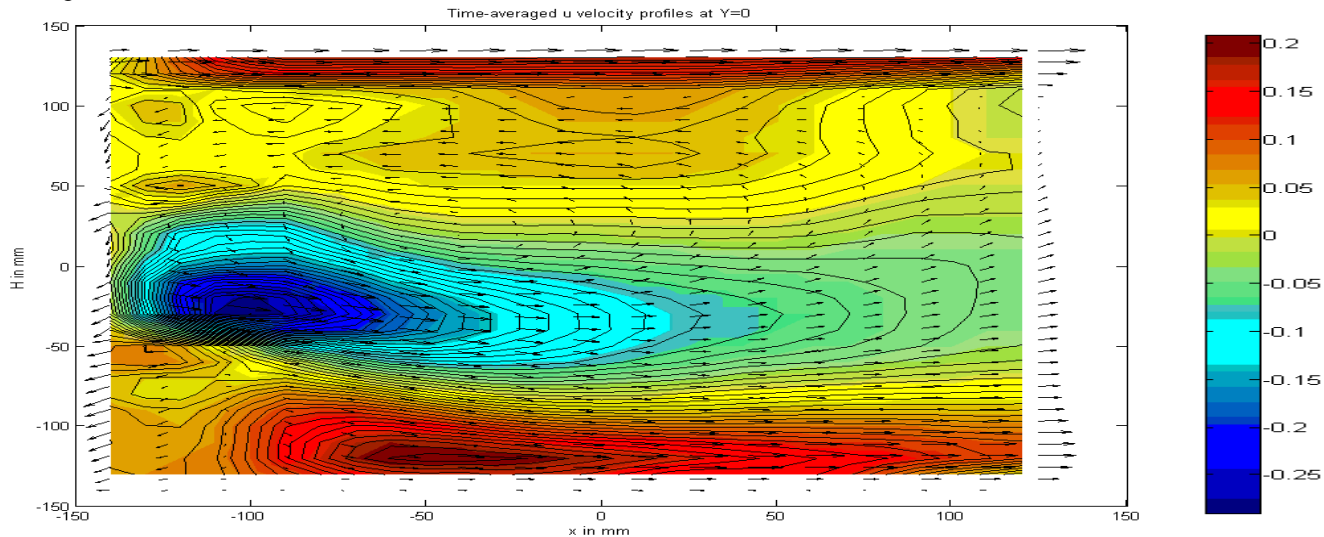


Figure 3-23. 3D vector statistics for directly behind the pile at LFP1F (ringed pile). The flow map is approximately 0.28 by 0.28m. The first three profiles from the left should be ignored as this is the location of the pile.

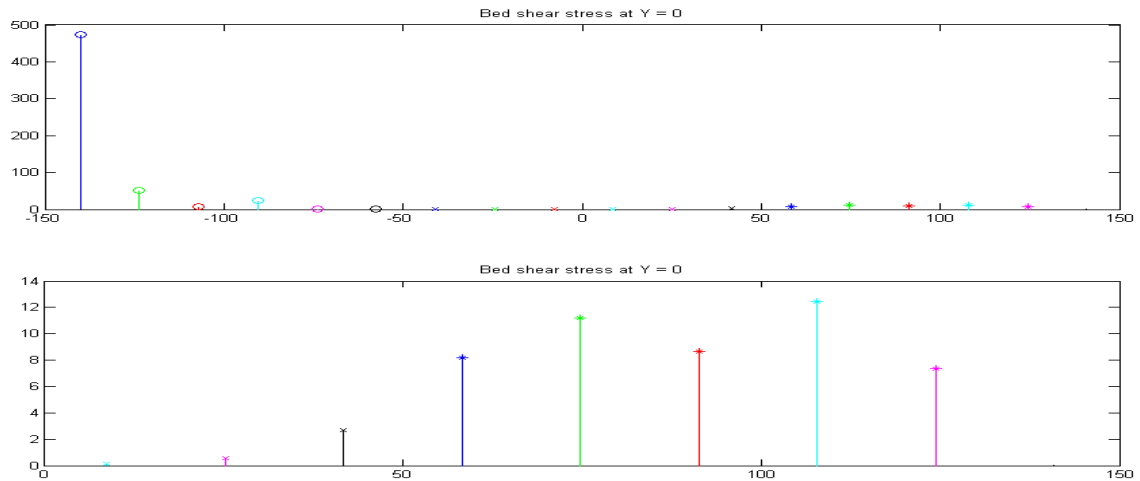


Figure 3-24a-b. Bed shear stress values at the bed relating to the equivalent profiles in figure 3-23 (figure 3-24a), directly behind the pile at LFP1E. In figure 3-24b the profiles after the point of separation only are displayed. These are the profiles that show logarithmic behaviour, and thus are the most likely to be approximately correct with the logarithmic method used. The first three values from the left of figure 3-24a should be ignored as this is the location of the pile.

NOTES

The above is merely the first results of the analysis of the data collected. The data collected is extensive (1TB), and the analysis process lengthy. Much of the data is still in Hull – where the processing tools are situated (parallel computing, and software). The first paper hoped to be submitted by the end of the year.

REFERENCES

- Adrian, R. J. (1991). "Particle Imaging Techniques for Experimental Fluid Mechanics." Annual Review of Fluid Mechanics **23**: 261-304.
- Ahmed, F., and Rajaratnam, N., (1998). "Flow around Bridge Piers." Journal of Hydraulic Engineering **124**(3): 288 - 300.
- Breusers, H. N. C., Nicollet, G., Shen, H. W., (1977). "Local Scour around Cylindrical Piers." Journal of Hydraulic Research **15**: 211 – 252.
- Chiew, Y. M. a. L., S. Y., (2002). "Protection of Bridge Piers using a Sacrificial Sill." Water and Maritime Engineering **156**(1): 53-62.
- Dargahi, B. (1987). Flow Field and Local Scouring around a Cylinder. Stockholm, Sweden, Royal Institute of Technology.
- Dey, S., Bose, S. K., Sastry, G. L. N., (1995). "Clearwater Scour at Circular Piers: A Model." Journal of Hydraulic Engineering **121**(12): 869 - 876.
- Dey, S., Raikar, R. V., (2007). "Characteristics of Horseshoe Vortex in Developing Scour Holes at Piers." Journal of Hydraulic Engineering **133**(4): 399 - 413.
- Escarameia, M. (1998). "Laboratory Investigation of Scour around Large Structures in Tidal Waters." Parallel Session (parallel45), 02.09.1998, 10:15 - 12:45.
- Ettema, R. (1980). Scour at Bridge Piers, University of Auckland.
- Graf, W. H., Istiarto, I., (2002). "Flow Pattern in the Scour Hole around a Cylinder." Journal of Hydraulic Research **40**(1): 13 - 20.
- Graf, W. H., Yulistiyanto, B., (1999). "Experiments on Flow around a Cylinder; the Velocity and Vorticity Fields." Journal of Hydraulic Research **36**(4): 637 - 654.

- Johnson, K. R., and Ting, F. C. K., (2003). "Measurements of Water Surface Profile and Velocity Field at a Circular Pier." Journal of Engineering Mechanics **129**(5): 502 - 513.
- Kumar, V., Ranga Raju, K. G., and Vittal, N., (1999). "Reduction of Local Scour around Bridge Piers using Slots and Collars." Journal of Hydraulic Engineering **125**(12): 1302 - 1305.
- Margheritini, L., Martinelli, L., Lamberti, A., Frigaard, P., (2006). Scour Around Monopile Foundation for Off=Shore Wind Turbine in Presence of Steady and Tidal Currents. Coastal Engineering.
- Melville, B. W. (1975). Local Scour at Bridge Sites. Auckland, Auckland University.
- Melville, B. W., and Coleman, S. E., (2000). Bridge Scour. Auckland, Water Resources Publications, LLC.
- Melville, B. W., and Raudkivi, R. J. (1977). "Flow Characteristics in Local Scour at Bridge Piers." Journal of Hydraulic Research **15**(4): 373 - 380.
- Roulund, A., Sumer, B. M., Fredsoe, J., and Michelsen, J., (2005). "Numerical and Experimental Investigation of Flow and Scour around a Circular Pile." Journal of Fluid Mechanics **534**: 351-401.
- Sarker, A. M. (1998). "Flow Measurement around Scoured Bridge Piers using Acoustic-Doppler Velocimeter (ADV)." Flow Measurement and Instrumentation **9**: 217-227.
- Shen, H. W., Schneider, V. R., and Karaki, S. S., (1969). "Local Scour Around Bridge Piers." JHD Proc. ASCE **95**(HY6): 1919 - 1940.
- Shen, H. W., Schneider, V. R., and Karaki, S. S., (1966). Mechanics of Local Scour. US department of Commerce, National Bureau of Standards, Institute of Applied Technology.
- Sumer, B. M., and Fredsoe, J., (1997). Scour Around a Large Vertical Circular Cylinder in Waves. 16th International Conference on Offshore Mechanics and Arctic Engineering. Yokohama, Japan.
- Sumer, B. M., and Fredsoe, J., and Christiansen (1992). "Scour Around Vertical Pile in Waves." Journal of Waterway, Port, Coastal, and Ocean Engineering **117**(1): 15 - 31.
- Sumer, B. M., Fredsoe, J., (2001a). "Wave Scour around a Large Vertical Circular Cylinder." ASCE Journal of Waterway, Port, Coastal and Ocean Engineering **127**(3): 125 - 134.
- Sumer, B. M., Whitehouse, R. R. S., Torum, A., (2001). "Scour Around Coastal Structures: a Summary of Recent Research." Coastal Engineering **44**: 153-19.
- Whitehouse, R. J. S. (1998). Scour at Marine Structures. London, Thomas Telford.